ORIGINAL PAPER

Molecular dynamics simulations of Nafion and sulfonated polyether sulfone membranes. I. Effect of hydration on aqueous phase structure

Takahiro Ohkubo · Koh Kidena · Naohiko Takimoto · Akihiro Ohira

Abstract We measured the water uptakes and proton conductivities of a Nafion membrane and three sulfonated polyether sulfone membranes (SPESs) with different values of ion-exchange capacity (IEC=0.75, 1.0 and 1.4 meq/g) in relation to relative humidity in order to apply the findings to polymer electrolyte membrane fuel cells. The number of water molecules per sulfonic acid group λ at each humidity level was independent of the relative humidity for all membranes, but the proton conductivities of the SPESs were inferior to that of Nafion for the same λ value. Classical molecular dynamics simulations for the same membranes were carried out using a consistent force field at λ=3, 6, 9, 12 and 15. The structural properties of water molecules and hydronium ions at a molecular level were estimated from radial distribution functions and cluster size distributions of water. We found that the radial distribution function of S(sulfonic acid)–S(sulfonic acid) of Nafion at λ=3 indicated a significant correlation between the S–S pair, due to water channels, while the S–S pair of the SPESs showed a poor correlation. The cluster size distribution of water was also calculated in order to estimate the connectivity of the water channel. It is clear that some water is present in the SPESs as small, isolated clusters, especially when the water content is low.

T. Ohkubo · K. Kidena · N. Takimoto · A. Ohira
FC-Cubic, National Institute of Advanced Industrial Science and Technology (AIST),
2-41-6 Aomi, Koto-ku,
Tokyo 135-0064, Japan

Present Address:
T. Ohkubo (✉)
Graduate School of Science and Technology, Chiba University, Inage-ku,
Chiba 263-8522, Japan
e-mail: ohkubo.takahiro@faculty.chiba-u.jp

Introduction

Proton exchange membranes (PEMs) are currently attracting considerable interest due to their potential use in PEM fuel cells (PEMFCs) [1]. Many studies on the development of new materials and investigations of the proton transport mechanisms in PEM have been conducted with the goal of realizing practical PEMFCs [2–5]. To date, characteristic parameters such as proton conductivity [6–10], gas permeability [11–15] and degradation rate [16–18] have been primarily studied for perfluorinated ionomers consisting of poly(tetrafluoroethylene) backbones with perfluorinated pendant chains terminated by sulfonic acid. Although perfluorinated membranes are good proton conductors, there are several problems associated with the use of these materials as PEMs of fuel cells: high cost, low operating humidity limit, and relatively high gas permeability. Therefore, the search for improved PEM materials continues.

Sulfonated hydrocarbon polymers such as polysulfones [19], polyimides [20], poly(ether ketone)s [21], etc. [22] have been developed as alternatives to perfluorinated membranes due to their good mechanical properties, thermal stability, and proton conductivity. The initial motivation for their development was mainly to mimic the properties of the perfluorinated membrane with low-cost alternatives; however, it has become clear that the distinct chemical and microstructural properties of these materials have great potential.

On the other hand, Nafion, which was commercialized by DuPont, is considered to be a typical representative of a perfluorinated ionomer membrane. Several excellent reviews

of perfluorinated ionomers [23–25] have been published that relate the present understanding of the morphology and complex molecular-level proton transport mechanisms associated with proton conductivity. The morphological properties of the water channels in perfluorinated membranes characterized by microphase separation have been primarily studied using small-angle scattering of neutrons and X-rays [26–29]. The existence of a small-angle scattering peak has been attributed to spherical reverse micelles of water domains, the so-called water channels, which form a network of water clusters on the nanometric scale. Accordingly, a better understanding of water channels is required in order to design new membranes for hydrocarbon polymers.

In recent years, the use of predictive computational modeling techniques has been found to be highly useful. For example, theoretical studies of the mechanisms of proton transport in perfluorinated ionomer membranes based on ab initio calculations have been performed [30–33]. In addition, the structural features of the hydrated membrane, including its morphology and dynamic properties, have been demonstrated by molecular dynamics (MD) [34–40] simulations in order to explore the conformational space at finite temperatures. Although MD simulations neglect the effects of the proton transport process based on proton sharing that occurs in aqueous solution, referred to as the Grotthuss mechanism, it is well suited to characterizing the water channels and transport in PEM. Urata et al. used an explicit all-atom description of a fully ionized sulfonic acid on the side chain, with torsional potentials and partial atomic charges calculated using hybrid DFT and MO theory [41]. They found the expected phase-separated structure, in which the dynamics of water molecules were highly restricted at low hydration levels due to strong interactions with SO_3^-. In a more recent study, Cui et al. investigated the morphology of hydrated Nafion based on the quantitative cluster size distribution as a function of water content [34]. They indicated that the cluster size distribution displayed distinctive differences in connectivity relating to the water channel between low and high hydration levels.

This paper shows the results of experimental measurements of water uptake and proton conductivity for Nafion and sulfonated polyether sulfone membranes (SPESs) in relation to the relative humidity. In order to characterize these experimental results, we also report the results of MD simulations of the same membranes used in the water uptake and proton conductivity measurements. High-performance polymers such as aromatic sulfonated poly (arylene ether sulfone) copolymers (BPSHs) [42–47] that are based on the backbone of SPES have been developed. Therefore, an understanding of SPESs at the molecular level would be useful for developing new materials. The significance of this work for Nafion is that although MD simulations of Nafion have already been used to determine

the morphological and dynamical properties of water, the results were slightly dependent on the molecular modeling methods and functional forms of the force fields used. For this reason, we performed MD simulations of Nafion to conduct a comparison with the reliable results obtained using the same modeling method as used for the SPESs.

During molecular modeling, particular attention should be paid to the ion-exchange capacity (IEC) of SPES and the water content, which are well known to be the parameters that determine proton conductivity. Based on these parameters, the morphologies of water molecules and hydronium ions in Nafion and the SPESs are explored via configuration snapshots, radial distribution functions, and cluster size distributions of water molecules. These results will be helpful when attempting to understand the specific features of PEMs that lead to enhanced performance.

Experimental and computational methodology

Water uptake and proton conductivity measurements

Commercially available perfluorinated Nafion membranes (NR-212) were purchased from DuPont and used as received. Hydrocarbon-type polymer membranes (SPES) with three different IEC values (0.75, 1.0 and 1.4 meq/g) were obtained from Sumitomo Chemical Co., Ltd. The IEC values of the SPESs were determined by titration.

Water uptake and proton conductivity were measured using an isotherm absorption measurement system (MSB-AD-V-FC, BEL Japan Inc.) equipped with an impedance analyzer (Solartron SI 1260). This system enabled simultaneous measurements of water uptake and proton conductivity in the same chamber. Each membrane sample was dried at 353 K for 1 h under dry nitrogen, then exposed to a humidified nitrogen environment at 313 K. When there was no further change in the weight of each sample, the sample weight and proton conductivity were measured sequentially. Humidity conditions were changed stepwise from 10 to 95% relative humidity (RH).

The water uptake of the membranes was calculated as the number of water molecules per sulfonic acid group, λ. Proton conductivity was measured using a four-point probe cell. An AC impedance spectrum was recorded over the frequency range from 10 Hz to 100 kHz using an impedance analyzer. Proton conductivity was calculated from the dry membrane thickness, and the membrane resistance was taken at the frequency that produced the minimum imaginary response.

Molecular modeling

The initial configurations of the molecular model for MD simulations were obtained as follows. For Nafion, a model oligomer based on that used in a past MD simulation study

[39] was employed to build a polymer chain, as shown in Fig. 1, with $x=12$. For the SPESs, monomers with and without sulfonated acid (AES and SAES), as shown in Fig. 2, were connected to build a polymer chain. The AES and SAES monomers were randomly introduced into the polymer chain to obtain the desired IEC values by setting the AES/SAES ratio appropriately. The AES/SAES ratios for the polymer chains were 60/12, 50/16 and 39/22, corresponding to IEC=0.75, 1.0 and 1.4 meq/g, respectively.

The molecular models used in the MD simulations were all-atom models. To maintain the neutrality of the system, H_3O^+ was used as the counterion to SO_3^-. The numbers of H_2O and H_3O^+ molecules and polymer chains are summarized in Table 1. In this simulation, the total number of particles was adjusted to about 15,000. The molecules and polymers were built with *MAPS* software (Scienomics SARL) [48]. Finally, the initial configuration of the polymer–hydronium–water system was constructed using Amorphous Builder in the *MAPS* software package. The density of the bulk system, which was used as input data for Amorphous Builder, was set to the experimental value of the dry density listed in Table 1.

Force field

The force field selected for this study is a simplified consistent force field (CFF), which is a second-generation force field [49] similar to COMPASS [50]. It has been extensively parameterized for common molecules and can provide an excellent potential model for polymers such as sulfonated poly(phenyl sulfone)s [51] and sulfonated polyimide copolymer [52] that contain water. The form of the function of the simplified CFF-type force field used here is

$$
\begin{aligned}
E = &\sum_b \left[k_2(b-b_0)^2 + k_3(b-b_0)^3 + k_4(b-b_0)^4 \right] \\
&+ \sum_\theta \left[k_2(\theta-\theta_0)^2 + k_3(\theta-\theta_0)^3 + k_4(\theta-\theta_0)^4 \right] \\
&+ \sum_\phi \left[k_1(1-\cos\phi) + k_2(1-\cos 2\phi) + k_3(1-\cos 3\phi) \right] \\
&+ \sum_\chi k_2\chi^2 + \sum_{b,b'} k(b-b_0)(b'-b'_0) \\
&+ \sum_{b,\theta} k(b-b_0)(\theta-\theta_0) + \sum_{i<j} \varepsilon_{ij} \left[2\left(\frac{r_{ij}^0}{r_{ij}}\right)^9 - 3\left(\frac{r_{ij}^0}{r_{ij}}\right)^6 \right] \\
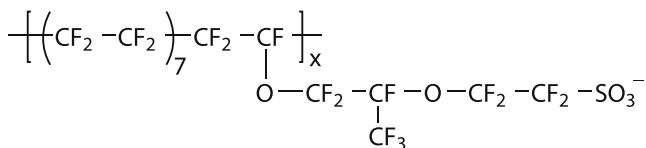&+ \sum_{i<j} \frac{q_i q_j}{r_{ij}}.
\end{aligned}
$$

(1)

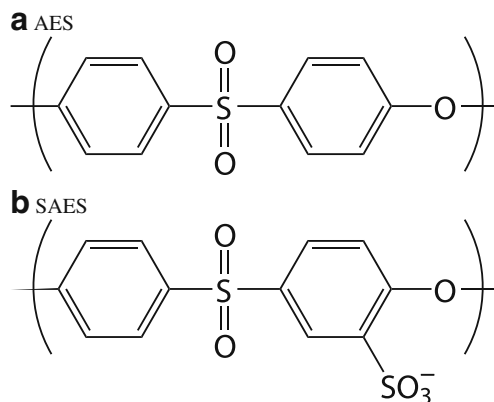Fig. 1 Chemical structure of the Nafion ionomer

Fig. 2 a–b Chemical structures of the monomers used to build the SPES polymers in simulations. a AES without sulfonic acid; b SAES with sulfonic acid

The functions can be divided into two categories: valence terms, including coupling and cross-coupling terms, and nonbonding interaction terms. The valence terms represent the internal coordinates of the bond (b), the angle (θ), the torsion angle (ϕ) and the out-of-plane angle (χ), while the cross-coupling terms bond–bond (b, b') and bond–angle (b, θ) include combinations of two or three internal coordinates. Nonbonding interactions, which include a LJ-9-6 function for the van der Waals (vdW) term and the coulombic function for the electrostatic interaction, are used. The LJ-9-6 parameters (ε and r^0) are given for like-atom pairs. For unlike-atom pairs, the sixth-order combination law is used to calculate the parameters:

$$
\begin{aligned}
r_{ij}^0 &= \left(\frac{(r_i^0) + (r_j^0)}{2} \right)^{1/6} \\
\varepsilon_{ij} &= 2\sqrt{\varepsilon_i \varepsilon_j} \left(\frac{(r_i^0)^3 (r_j^0)^3}{(r_i^0)^6 + (r_j^0)^6} \right).
\end{aligned}
$$

(2)

The electrostatic interaction is represented by employing atomic partial charges as the last term in Eq. 1.

The polymer–hydronium–water system was fragmented in order to assign the force field parameters using the *Direct Force Field* software (Aeon Technology, Inc.) [53]. Although most of the fragments of the system can be assigned force field parameters using the CFF force field database in *Direct Force Field*, the parameters of H_3O^+ and the fragments that included the sulfonic acid groups in the SPESs and Nafion (as shown in Fig. 3) were missing. Therefore, we developed new force field parameters. The procedure used to calculate the force field parameters followed the method developed by Sato et al. [54].

For the hydronium ion and fragments shown in Fig. 3, the MO calculations were carried out using the *Gaussian03* software package. The geometry was fully optimized in order to characterize the minimum energy structure. Two

Table 1 Numbers of H₂O and H₃O⁺ molecules and polymer chains used in the simulated systems. λ and ρ_c denote the number of water molecules per sulfonic acid group and the calculated bulk density (g/cm³) of the equilibrated systems described in "Molecular dynamics simulations." IEC (meq/g) and dry density (ρ_{dry}; g/cm³) values are also listed

| Nafion (ρ_{dry}=1.95)					
λ	Number of chains	H₃O⁺	H₂O	Total number of particles	ρ_c
3	16	192	384	15008	1.99
6	14	168	840	14644	1.93
9	13	156	1248	15002	1.86
12	12	144	1584	15144	1.81
15	11	132	1848	15070	1.75
SPES (IEC=0.75, ρ_{dry}=1.31)					
3	16	96	192	15104	1.34
6	15	90	450	14970	1.35
9	15	90	720	15780	1.35
12	14	84	924	15484	1.35
15	13	78	1092	15080	1.34
SPES (IEC=1.0, ρ_{dry}=1.28)					
3	17	136	272	15266	1.36
6	16	128	640	15520	1.37
9	15	120	960	15630	1.36
12	14	112	1232	15596	1.35
15	13	104	1456	15418	1.34
SPES (IEC=1.4, ρ_{dry}=1.24)					
3	17	187	374	15521	1.38
6	15	165	825	15180	1.38
9	14	154	1232	15554	1.37
12	13	143	1573	15587	1.35
15	12	132	1848	15576	1.33
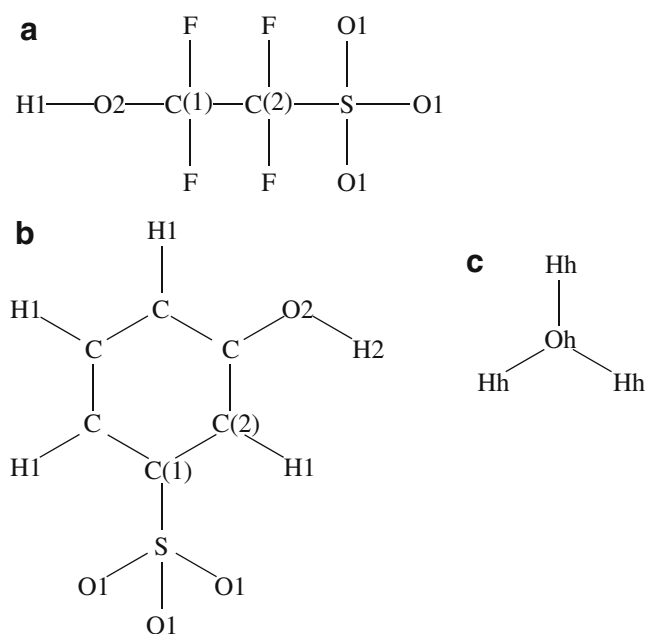
Fig. 3 a–c Three fragments missing from the CFF force fields database in *Direct Force Field*: **a** sulfonic acid group of Nafion; **b** sulfonic acid group of SPES; **c** hydronium. Estimated force field parameters corresponding to the assigned atom type are listed in the "Appendix"

fragments that included a sulfonated acid to model the Nafion and the SPESs were optimized at the B3LYP/6-311G** level, and the hydronium ion was optimized at the B3LYP/6-311G* [55–58] level. Total energies, analytical gradients and Hessian matrices were calculated in order to prepare the data for parameterization of the force field. In addition, the conformational structure had to be sampled in order to generate a high-quality force field. Distorted structures where the dihedral angle of interest was fixed at selected values to sample conformational spaces were also calculated. Partial atomic charges were obtained by fitting the ab initio electrostatic potential surfaces (electrostatic potential fitted, ESP, method) [59]. The evaluated force field parameters and partial charges corresponding to the assigned atoms in Fig. 3 are summarized in the "Appendix."

Molecular dynamics

We performed MD simulations with the LAMMPS code (http://lammps.sandia.gov) from Plimpton at Sandia [60]. Equations of motion were integrated using the Verlet algorithm [61] with a time step of 1.0 fs, and the particle–particle particle–mesh (PPPM) method [62] was employed to calculate electrostatic interactions. For each system, the MD simulation was performed at 313.15 K, which is the

same as the temperature at which the water uptake and proton conductivity measurements were performed. The simulations were performed as follows: first the systems were equilibrated for 1 ns with a step of 1 fs using the NVT ensemble (fixed volume and Nose–Hoover thermostat [63–66]). This was followed by a 15 ns MD simulation using the NPT ensemble (fixed pressure at 101,325 Pa and Nose–Hoover thermostat). The trajectories obtained from the last 5 ns of the NPT ensemble every 5 ps were used to compute the structural properties.

Results and discussion

Water uptake and conductivity

The water uptakes λ of Nafion and the SPESs with different IECs (0.75, 1.0 and 1.4 meq/g) at 313.15 K are shown as a function of the relative humidity in Fig. 4. The water uptake accelerates above about 70% RH for all membranes. The hydration behavior as a function of relative humidity is almost the same for all membranes in terms of λ. On the other hand, the dependence of the proton conductivity on the relative humidity clearly differs among the membranes, as shown in Fig. 5. The proton conductivities for the SPESs are not plotted at a low relative humidity, due to the lower detection limit in Fig. 5. The proton conductivities of the SPESs are about a hundred or a thousand times less than that of Nafion for the same λ. In particular, the SPES membranes exhibit poor proton conductivities at low humidity; that is, the dependence of the proton conductivity on the water content for the SPESs is much stronger than it is for Nafion. Regarding the dependence of the proton
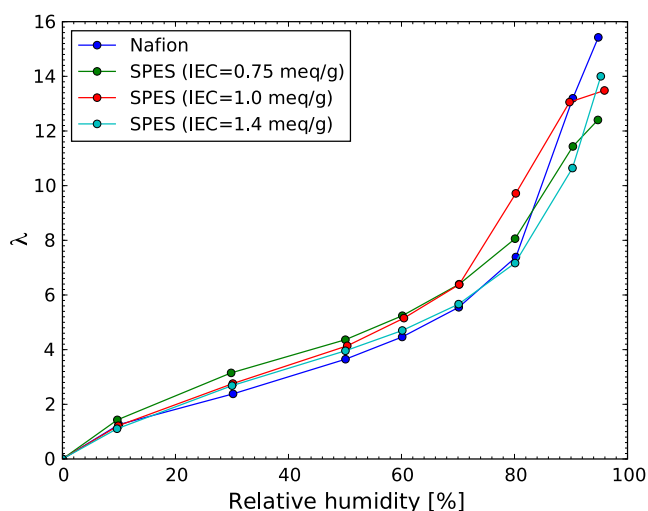

Fig. 4 Number of water molecules per sulfonic acid group λ for Nafion and the SPESs (IEC=0.75, 1.0 and 1.4 meq/g) as a function of relative humidity at 313 K
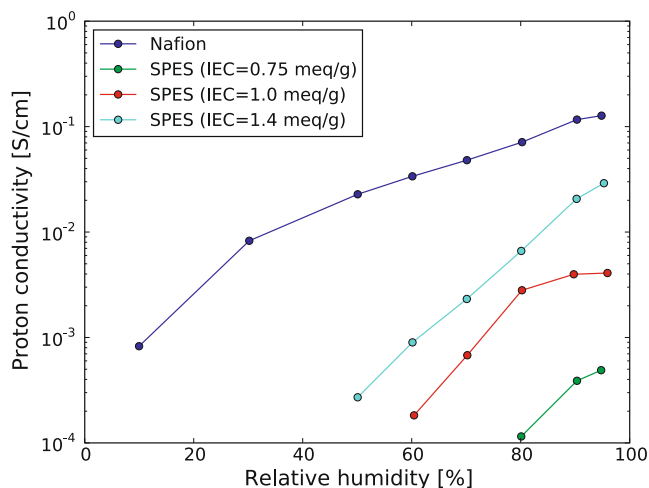

Fig. 5 Proton conductivity of Nafion and the SPESs (IEC=0.75, 1.0 and 1.4 meq/g) as a function of relative humidity at 313 K

conductivities of the SPESs on the IEC, higher proton conductivities were achieved with a higher IEC at the same humidity.

These results for water uptake and proton conductivity as a function of relative humidity strongly attracted our interest, and the question of how Nafion and the SPESs differ at the molecular level was particularly interesting. Therefore, we sought to explain these results at the molecular level based on the structures of the water channels obtained from MD simulations.

Molecular dynamics simulations

The calculated bulk densities are listed in Table 1. For all membranes, the bulk densities decreased with increasing λ, which means that the membranes swell upon hydration.

Various analyses of the structural properties of Nafion and the SPESs at the molecular level were carried out using the configuration snapshots obtained from the MD simulations. The parameters analyzed were the radial distribution functions and the cluster size distribution of water.

Snapshots of the equilibrating configurations of Nafion and the SPESs with λ=3, 9, and 15 at the final time step are displayed using Visual Molecular Dynamics (VMD) [67] in parts a–d of Fig. 6. Blue lines denote the periodic boundaries of the unit cell. Gray lines, yellow balls, blue balls, sky blue balls and white balls correspond to the polymer backbone, sulfur (sulfonic acid group), oxygen (water), oxygen (hydronium) and hydrogen (water and hydronium), respectively. For all membranes, at λ=3, H_2O and H_3O^+ are only located around SO_3^- at uniformly dispersed positions in the cell. Wide water channels with enhanced connectivity are observed with increasing λ for all membranes.

In a rough comparison of Nafion and the SPESs, the SPESs exhibit more disperse and narrower water channels

Fig. 6 a–d Final snapshots of **a** Nafion, **b** SPES with IEC= 0.75 meq/g, **c** SPES with IEC= 1.0 meq/g, and **d** SPES with IEC=1.4 meq/g at λ=3, 9 and 15. *Gray lines*, polymer backbone; *yellow ball*, sulfur of sulfonic acid group; *blue ball*, oxygen of water; *sky-blue ball*, oxygen of hydronium; *white ball*, hydrogen of water and hydronium. *Blue lines* are periodic boundaries of the unit cell
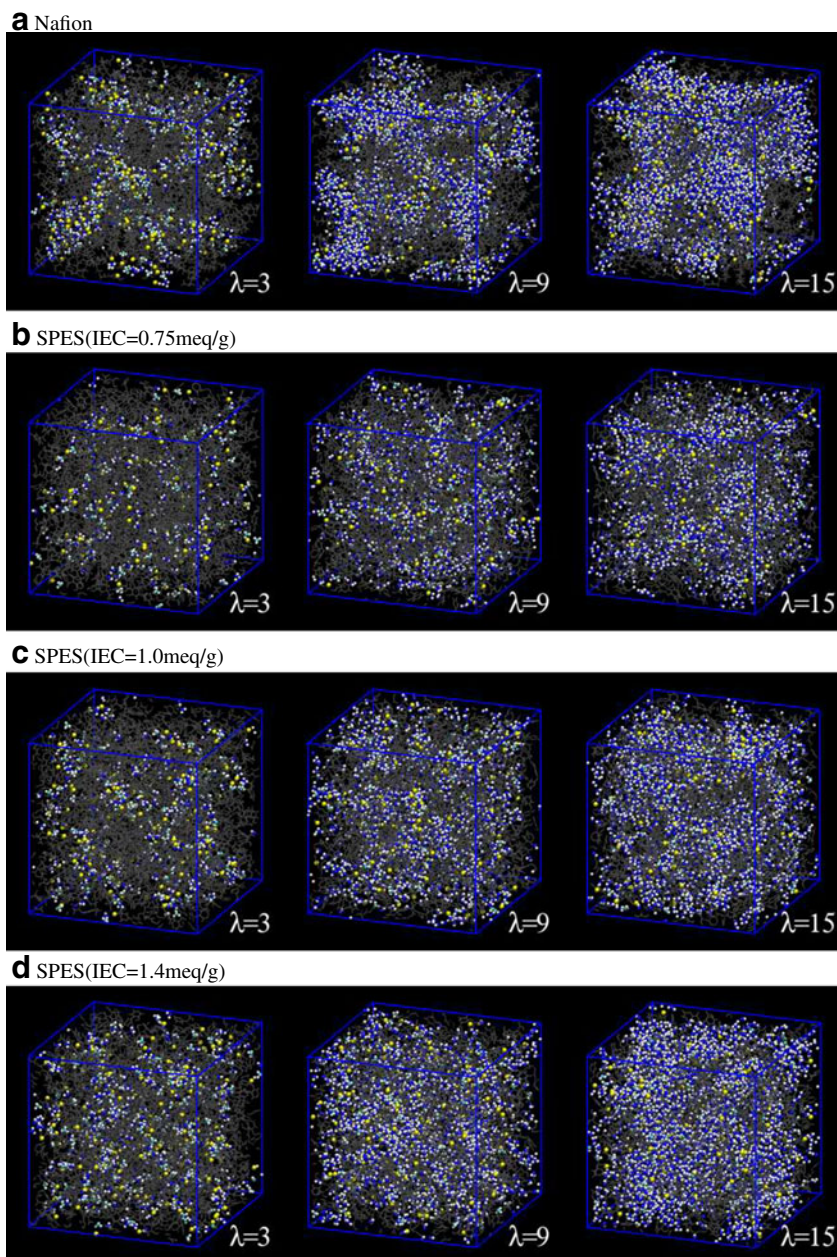
than those of Nafion at the same λ. However, a more quantitative assessment of the structures of the water channels can be achieved through other analyses.

Radial distribution functions

The radial distribution function (RDF) $g(r)$ is defined as the probability of finding an atom B at a distance r from a reference atom A, averaged over the trajectories, and is written as

$$g_{A-B}(r) = \left(\frac{n_B}{4\pi r^2 dr}\right) \bigg/ \left(\frac{N_B}{V}\right), \qquad (3)$$

where n_B is the number of B atoms located at a distance r in a shell with thickness dr from atom A, while N_B and V are the total number of B atoms and the total volume of the system, respectively.

Figure 7 shows the sulfonic acid sulfur to sulfonic acid sulfur (S–S) RDFs for different hydration levels of λ=3, 6, 9, 12 and 15. In the case of Nafion, the RDF at λ=3 has two peaks, occurring at approximately 4.7 and 7.1 Å. These peaks are broad and become weaker with increasing λ. At λ=15, these peaks are almost flattened out to 1.0, since the polymer chains become more flexible at high hydration levels and the S–S correlation is eroded by the strong electrostatic interaction between the SO_3^- groups. The S–S
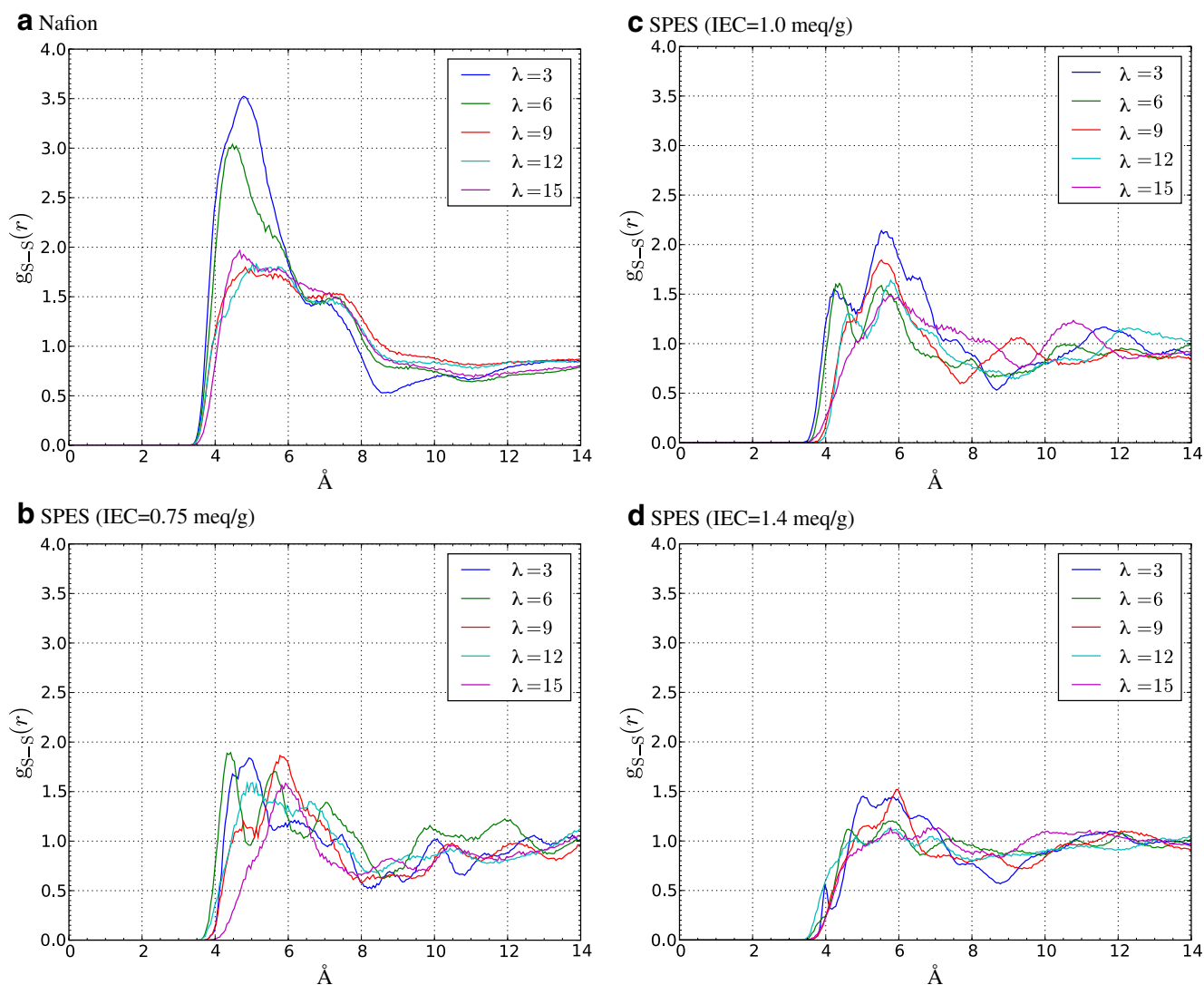
Fig. 7 **a–d** Sulfur(sulfonic acid)–sulfur(sulfonic acid) radial distribution functions for Nafion and the SPESs (IEC=0.75, 1.0 and 1.4 meq/g) at λ=3, 6, 9, 12 and 15: **a** Nafion; **b** SPES with IEC=0.75 meq/g; **c** SPES with IEC=1.0 meq/g; **d** SPES with IEC=1.4 meq/g

RDFs of the SPESs are more complex than those of Nafion and change continuously as a function of λ. The S–S RDFs of the SPESs have incoherent peak positions for all λ, although weak peaks occurring at approximately 4.3 and 5.7 Å were found. A decrease in peak height with increasing water uptake was also observed. In particular, the S–S correlation in the range of 4–5 Å disappears at high λ. As in the case of Nafion, it is expected that increasing the amount of water promotes polymer chain flexibility, which releases the constraints on the S–S correlation. A distinct difference between the S–S RDFs of Nafion and the SPESs is the presence of an intense peak at low λ. As reported from ab initio calculations by Paddison and Elliott [68, 69], the Nafion oligomer has a minimum binding energy per water molecule for a structure with a kink in the backbone, which allows the SO_3^- groups to come into close proximity.

Since the kinked backbone of Nafion at low λ can efficiently bind H_2O with SO_3^-, a strong S–S correlation is observed in the S–S RDF of Nafion. On the other hand, the number of degrees of freedom for SO_3^- in the SPESs is clearly less than it is in Nafion, due to the absence of the side chain. As a result, the S–S RDFs show poor correlation at low λ.

The sulfonic acid sulfur to water oxygen (S–Ow) RDFs are presented in Fig. 8. For all membranes, the S–Ow RDFs show a strong first peak at approximately 3.9 Å and a second peak at around 6.2 Å. The height of the first peak gradually decreases with increasing hydration. The behavior of the first peak as a function of λ is similar for Nafion and the SPESs; that is, the behavior of the local coordination structure of H_2O around SO_3^- does not differ greatly between Nafion and the SPESs. With regards to the
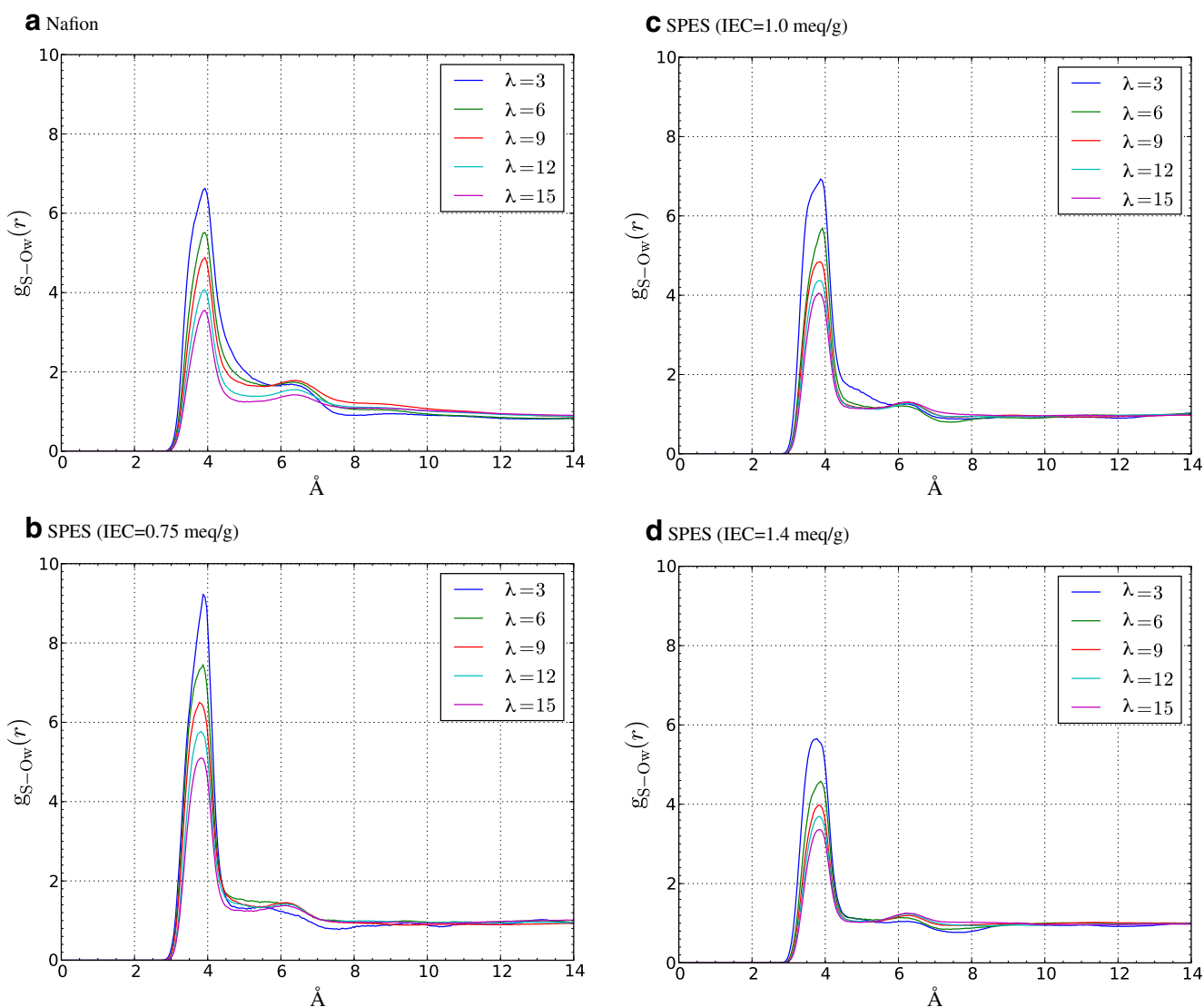
Fig. 8 **a–d** Sulfur(sulfonic acid)–oxygen(water) radial distribution functions for Nafion and the SPESs at λ=3, 6, 9, 12 and 15: **a** Nafion; **b** SPES with IEC=0.75 meq/g; **c** SPES with IEC=1.0 meq/g; **d** SPES with IEC=1.4 meq/g

IEC dependence of SPES, increasing the IEC decreases the peak height at constant λ.

Figure 9 shows the sulfonic acid sulfur to hydronium oxygen (S–Oh) RDFs. For Nafion, the highest peak for each value of λ was observed at 4 Å. The first peak height of S–Oh was higher than that of S–Ow. The strong electrostatic interaction between H_3O^+ and SO_3^- was expected considering the positive charge of H_3O^+ and the negative charge of SO_3^-. There is also a weak second peak at around 6.2 Å that corresponds to solvent (water) separated ion pairs. The S–Oh RDFs of the SPESs have a split first peak at approximately 3.4 and 4.9 Å at low λ. The splitting of the first peak is likely due to the strong interaction of H_3O^+ with SO_3^-, which is the configuration of positively charged $S(SO_3^-)$, negatively charged

$O(SO_3^-)$, positively charged $H(H_3O^+)$ and negatively charged $O(H_3O^+)$ caused by electrostatic interactions. At high water contents, the interaction between H_3O^+ and SO_3^- weakens compared to its strength at low water contents. High levels of H_2O at high λ can cause a relaxation of the local configuration of H_3O^+ around SO_3^-. Another unique feature of the S–Oh RDF for the SPESs is the dependence of the peak height on λ, which is smaller than that of Nafion. This means that the number of H_3O^+ molecules that are separated from SO_3^- in the SPESs does not increase with increasing hydration.

The RDFs of hydronium oxygen to water oxygen (Oh–Ow) for different levels of hydration are shown in Fig. 10. For all membranes, a first peak is noted at 2.8 Å and a weak second peak at about 5.2 Å. A slight peak at approximately
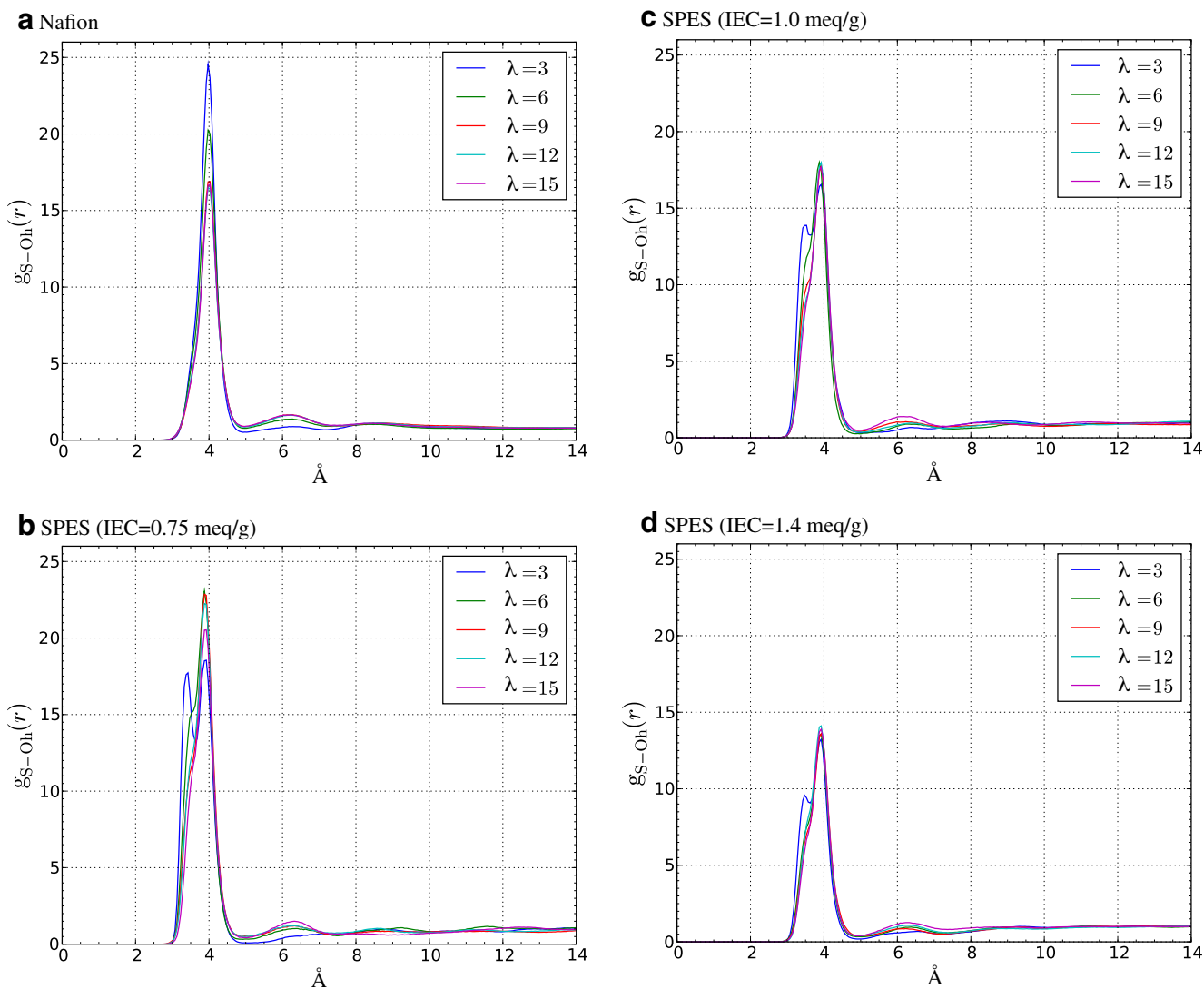
a Nafion

b SPES (IEC=0.75 meq/g)

c SPES (IEC=1.0 meq/g)

d SPES (IEC=1.4 meq/g)

Fig. 9a–d a–d Sulfur (sulfonic acid)–oxygen (hydronium) radial distribution functions of Nafion and the SPESs at λ=3, 6, 9, 12 and 15: **a** Nafion; **b** SPES with IEC=0.75 meq/g; **c** SPES with IEC=1.0 meq/g; **d** SPES with IEC=1.4 meq/g

7.2 Å was also observed in the Oh–Ow RDF. For all membranes, the trend for the Oh–Ow RDF with hydration is that the height of the first peak decreases with increasing λ. This behavior suggests that the binding of H_2O to H_3O^+ decreases due to the solvent effect with increasing water. Moreover, the Oh–Ow RDFs of the SPESs are less dependent on IEC, suggesting that the solvating ability of water to dissociate H_3O^+ is independent of IEC.

To obtain further information regarding the presence of water molecules in the vicinity of the sulfonic acid group, the hydration number can be obtained by plotting the average number of water molecules present within a shell of a certain radius. Figure 11 shows the hydration numbers of H_2O and H_3O^+ around SO_3^- at λ=3, 6, 9, 12 and 15 as a function of distance, as calculated from Figs. 8 and 9. The trend for the hydration number as a function of λ is almost

the same for all membranes. With increasing λ, the hydration number of H_2O increases while the hydration number of H_3O^+ decreases. This result means that the solvent effect for the dissociation of H_3O^+ is considerable at high hydration levels. Comparing Nafion and the SPESs, the decreases in the hydration number of H_3O^+ from λ=3 to 15 within 4.5 Å are 1.5 (Nafion), 0.33 (SPES, IEC=0.75), 0.30 (SPES, IEC=1.0), and 0.52 (SPES, IEC=1.4). The solvent effect for SPES may be weaker than that for Nafion due to the higher partial charge of SO_3^-.

Cluster size distribution of water

In order to characterize the morphological features of the water channels, we calculated the cluster size distribution of water. In the evaluation, H_2O and H_3O^+ were not identified
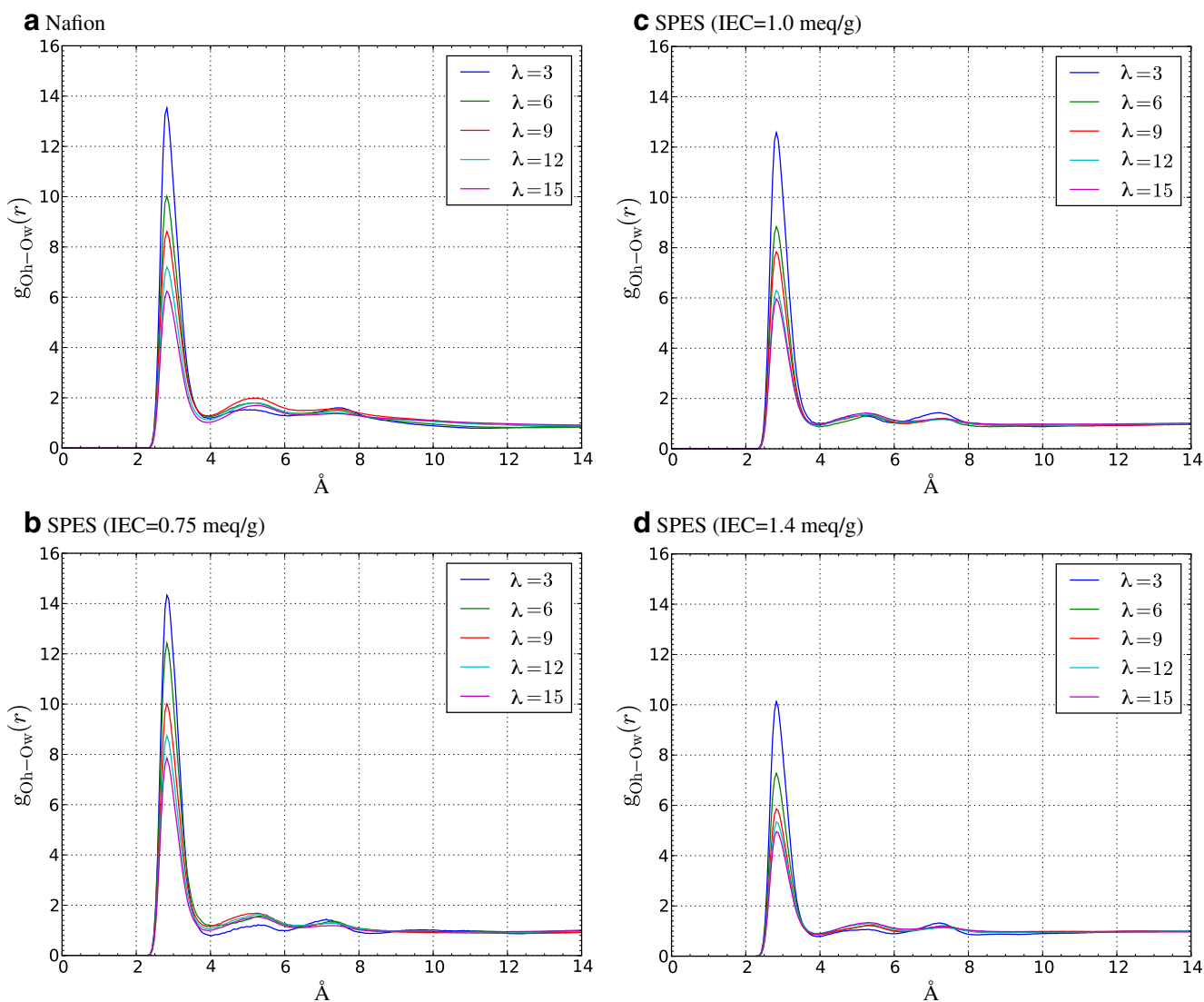
Fig. 10 a–d Oxygen(hydronium)–oxygen(water) radial distribution functions for Nafion and the SPESs at λ=3, 6, 9, 12 and 15: **a** Nafion; **b** SPES with IEC=0.75 meq/g; **c** SPES with IEC=1.0 meq/g; **d** SPES with IEC=1.4 meq/g

when counting the cluster size of water. The cluster size distribution was estimated by setting a cutoff distance that was used to determine whether individual molecules of H_2O or H_3O^+ belonged to the same cluster. The definition of the cutoff distance was arbitrary, although it is possible to compare cluster structures and estimate relative trends in any system. In this study, the cutoff distance was set at 3.5 Å for all systems, and this roughly includes all water molecules in the first hydration shell, based on water oxygen to water oxygen (not shown in the figure) and Oh–Oh RDFs (shown in Fig. 10). We calculated the time-averaged cluster size distributions of water, including hydronium ions, for Nafion and the SPESs with three IEC values. The cluster size distributions are presented in Fig. 12, where the cluster size is classified as either small (0–100; left) and large (>400; right), respectively.

The degree of connectivity of the water channels can be interpreted from the cluster size distributions corresponding to the snapshots in Fig. 6. The behavior of the cluster size distribution with increasing hydration is similar for all membranes: small clusters of less than 100 molecules decrease with increasing hydration. It is thought that isolated water in a small cluster cannot effectively contribute to proton transfer based on the proton-hopping mechanism (Grotthuss); that is, the presence of large clusters enhances proton conductivity. Water molecules belonging to large clusters were observed for hydration levels of more than λ=6 for Nafion, while water molecules in large clusters were observed for the SPESs at λ=12 for IEC=0.75 and λ=9 for IEC=1.0 and 1.4. Therefore, for the SPESs, water does not organize into large clusters as efficiently as it does for Nafion. Regarding the dependence
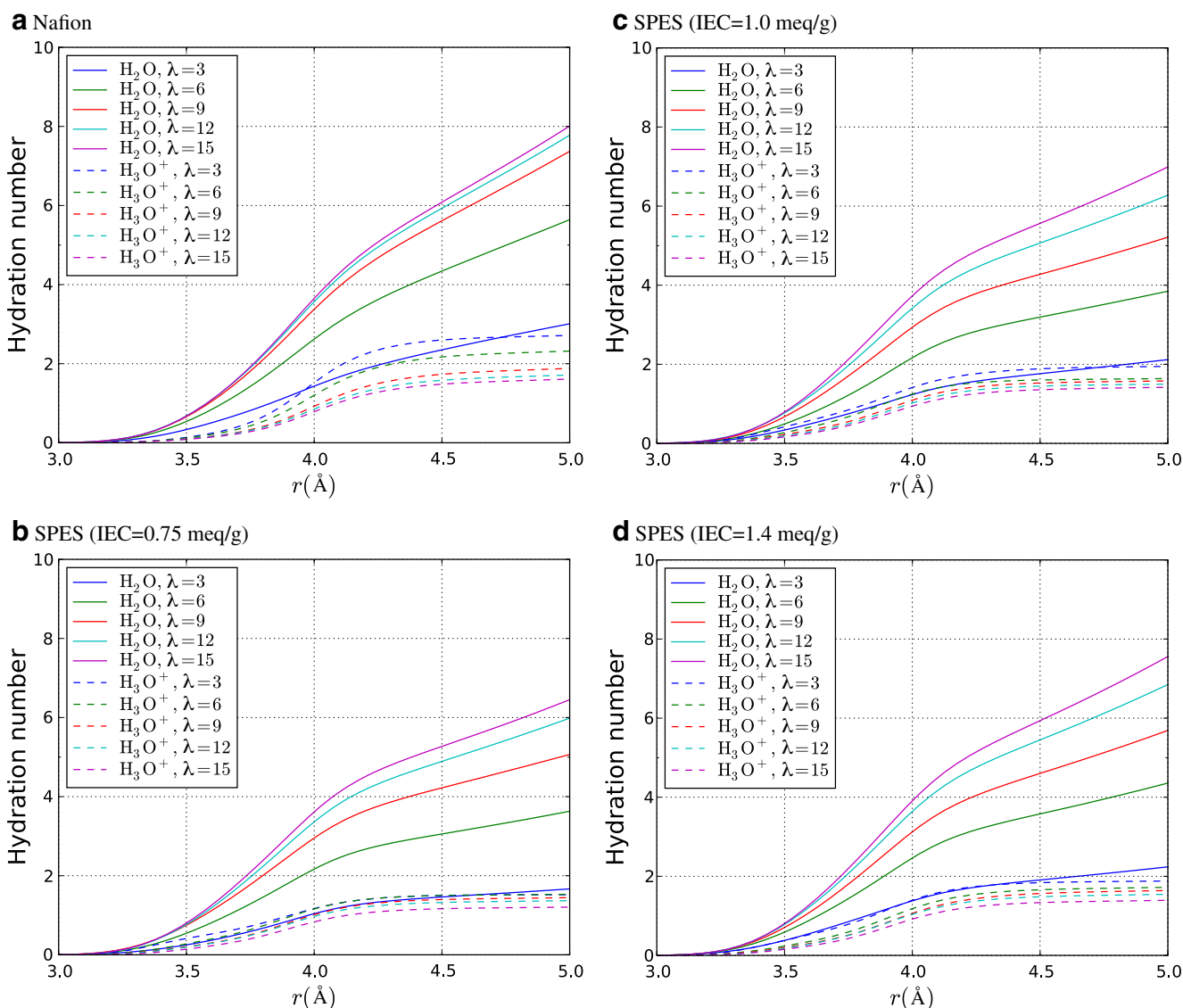
Fig. 11 a–d Number of water molecules and hydronium ions around a sulfonic acid group as a function of distance: **a** Nafion; **b** SPES with IEC= 0.75 meq/g; **c** SPES with IEC=1.0 meq/g; **d** SPES with IEC=1.4 meq/g at λ=3, 6, 9, 12 and 15. *Solid lines*, water; *dotted lines*, hydronium

of the SPESs on the IEC, large clusters form more easily with increasing IEC at a given λ. This agrees with observations of proton conductivity, and it is thought that the ease with which a large water cluster is formed is a key factor in obtaining high proton conductivity.

To compare the behavior of the cluster size distributions as a function of λ, the ratio of water molecules belonging to a large cluster was measured as a function of λ in Fig. 13. For Nafion, the clusters become large in the range λ=3 to 6, while for the SPESs, large clusters are formed at higher λ values than for Nafion. At λ=15, all of the water in Nafion and the SPES with IEC=1.4 belongs to a large cluster, while about 6% and 7% of the water is present in small clusters in the SPESs with IEC=0.75 and 1.0 meq/g, respectively. The isolated water molecules remain in the

small clusters due to the dispersed SO_3^-, regardless of the hydration level. It is likely that the location of the SO_3^- on the flexible side chain of Nafion is more advantageous to the formation of a large water cluster than the location of the SO_3^- on the main chains of the SPESs.

Conclusions

We measured the water uptakes and proton conductivities of Nafion and SPES (IEC=0.75, 1.0 and 1.4 meq/g) membranes under different relative humidity conditions. All membranes exhibited a similar λ dependence, but the proton conductivities were significantly different for all membranes. The Nafion membrane had the highest proton
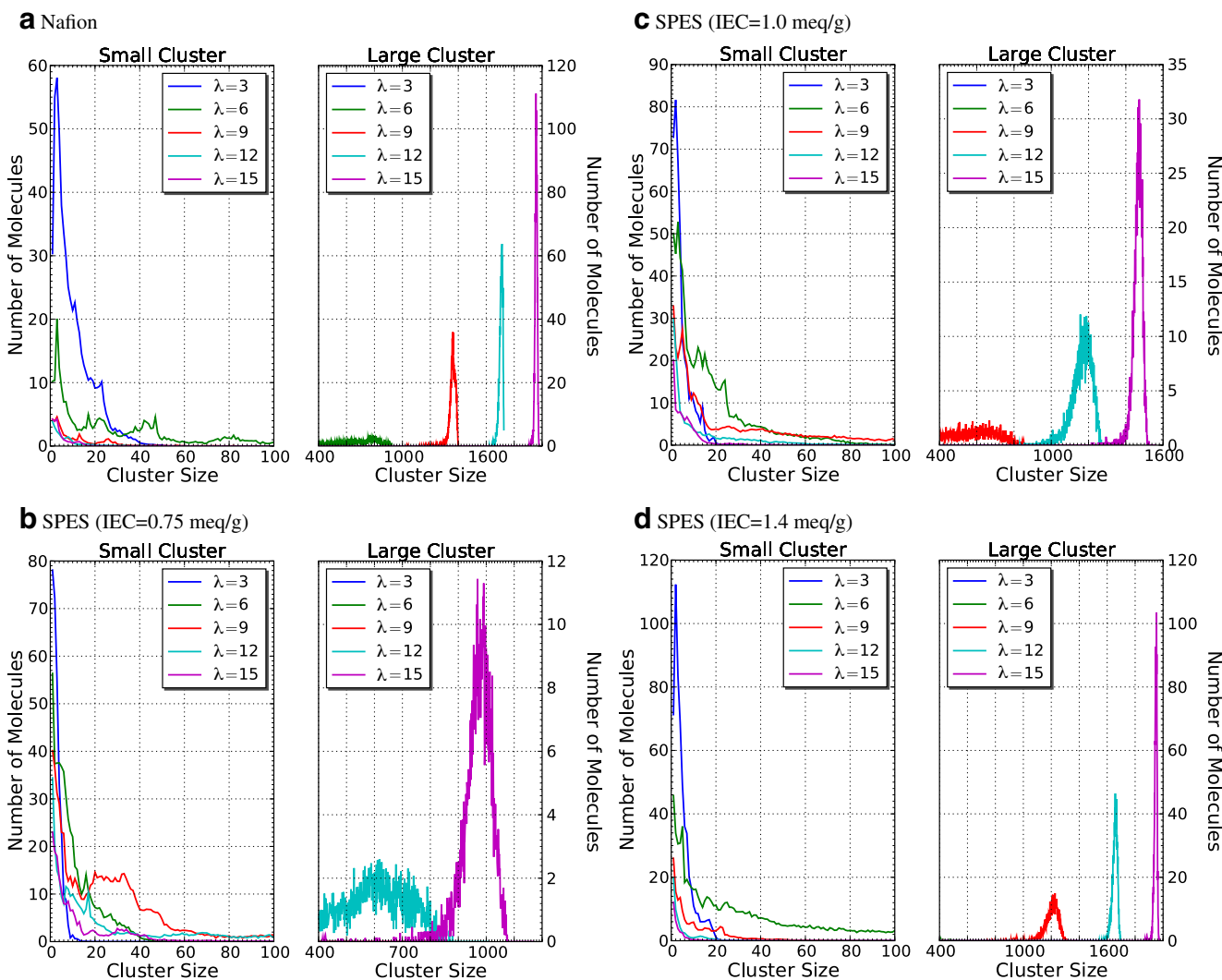
Fig. 12 a–d Cluster distributions of water for λ=3, 6, 9, 12 and 15, and based on a cutoff distance of 3.5 Å. **a** Nafion; **b** SPES with IEC= 0.75 meq/g; **c** SPES with IEC=1.0 meq/g; **d** SPES with IEC=1.4 meq/g
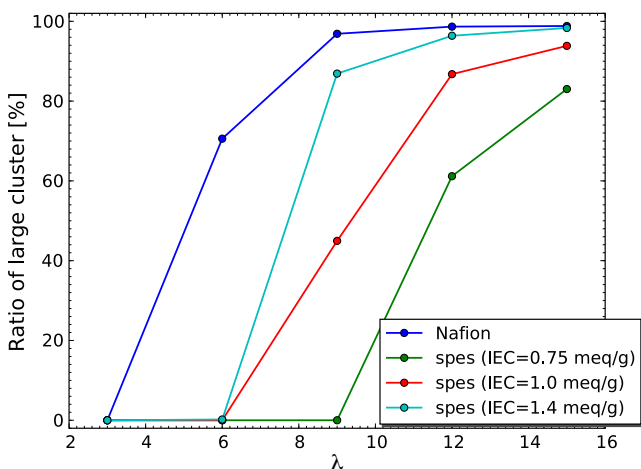
Fig. 13 Plot showing the ratio of water molecules in large clusters as a function of λ for Nafion and for the SPESs with IEC=0.75, 1.0 and 1.4 meq/g

conductivity, while the SPES membranes had poor conductivities, especially at lower humidity.

MD simulations of molecular models of Nafion and the SPESs (IEC=0.75, 1.0 and 1.4 meq/g) were also performed in order to study the morphological properties of the aqueous phases of the systems at the molecular level. In these simulations, the water uptake was set to λ=3, 6, 9, 12 and 15. Our calculations reproduced the geometric properties of the water channels related to proton conductivity reasonably well. One of the differences observed between the structure of the water channel in Nafion and those in the SPESs was the S–S RDFs. Nafion had two intense peaks at approximately 4.7 and 7.1 Å at λ=3, while the SPESs exhibited a poor correlation for S–S. The hydration structure of H_2O and H_3O^+ around SO_3^- was similar for all membranes, although the cluster size distributions differed considerably for each membrane. The ratio of

H$_2$O molecules in large clusters as a function of λ showed that most of the water in the SPESs only became incorporated into large clusters (thus enhancing conductivity) when the hydration level became sufficiently high.

Appendix

Force field parameters

Table 2 Developed CFF-type force field parameters for the Nafion fragment with a sulfonic acid group, as shown in Fig. 3a

Bond term	b_0	k_2	k_3	k_4
C–C	1.53790	346.66210	−693.32420	808.87820
C–O2	1.33780	499.62410	−999.24820	1165.78960
C–F	1.33190	459.19360	−918.38710	1071.45160
C–S	1.58630	160.73710	−321.47420	375.05330
H1–O2	0.97110	556.45060	−1112.90120	1298.38470
O1–S	1.45740	659.57790	−1319.15580	1539.01510
Angle term	θ_0	k_2	k_3	k_4
C–C–O2	114.18540	89.60260	−22.02940	−19.57050
C–C–F	118.50730	38.51610	−11.51040	−8.67540
F–C–O2	118.07370	106.04220	−31.10370	−23.80490
F–C–F	115.20590	76.93370	−19.84590	−16.91690
C–C–S	133.45650	45.38170	−24.25490	−11.99220
F–C–S	108.59770	58.20100	−10.66400	−12.32010
C–O2–H1	110.58730	67.07760	−13.74340	−14.34330
C–S–O1	91.08200	47.90880	−0.48900	−9.70980
O1–S–O1	125.42920	82.64350	−32.67930	−19.81820
Torsion term	k_1	k_2	k_3	
O2–C–C–S	0.00000	0.07560	1.62160	
F–C–C–O2	0.00000	1.27170	−0.90720	
F–C–C–S	0.00000	-0.17040	−0.54650	
F–C–C–F	0.00000	1.21400	0.21790	
C–C–O2–H1	0.00000	0.90850	0.05210	
F–C–O2–H1	0.00000	1.05270	−0.30560	
C–C–S–O1	0.00000	-0.32140	0.06920	
F–C–S–O1	0.00000	0.29780	−0.12300	
Bond–bond cross-coupling	k			
C–C–O2	40.42210			
C–C–F	19.72960			
F–C–O2	130.90110			
F–C–F	108.37370			
C–C–S	80.41830			
F–C–S	25.12490			
C–O2–H1	31.38040			
C–S–O1	−13.77650			
O1–S–O1	34.85110			
Bond–angle cross-coupling	k			
C–C–O2	59.87090			

Table 2 (continued)

Bond term	b_0	k_2	k_3	k_4
O2–C–C	68.43380			
C–C–F	22.82100			
F–C–C	62.40730			
O2–C–F	75.43300			
F–C–O2	102.67910			
F–C–F	71.46720			
C–C–S	58.67190			
S–C–C	−5.99960			
S–C–F	−38.56970			
F–C–S	65.33430			
C–O2–H1	64.36920			
H1–O2–C	38.44820			
C–S–O1	−79.79420			
O1–S–C	11.99060			
O1–S–O1	47.62750			
Lennard–Jones term	r_0	ε		
S	4.05960	0.22500		
O1	3.38640	0.15300		
O2	3.43740	0.15300		
C	4.00860	0.05940		
F	3.41290	0.05940		
H1	2.77440	0.02700		
Partial charge	q			
S	1.2820			
O1	−0.6821			
O2	−0.5978			
C(1)	0.6722			
C(2)	0.2622			
F	−0.2488			
H1	0.4182			

Table 3 Developed CFF-type force field parameters for the SPES fragment with a sulfonic acid group, as shown in Fig. 3b

Bond term	b_0	k_2	k_3	k_4
C–O2	1.40910	321.92150	−643.84290	751.15010
H2–O2	0.96800	577.62060	−1155.24120	1347.78140
C–C	1.36520	512.58710	−1025.17410	1196.03650
C–S	2.03160	67.42910	−134.85820	157.33460
C–H1	1.09770	363.23820	−726.47640	847.55580
O1–S	1.46760	616.74020	−1233.48040	1439.06050
Angle term	θ_0	k_2	k_3	k_4
C–O2–H2	103.80180	68.43840	−9.12320	−14.20250
C–C–O2	106.39280	50.47010	−8.07080	−10.57830
C–C–C	119.33440	59.32040	−18.36260	−13.44970
C–C–S	108.85380	83.52340	−15.53360	−17.70220
C–C–H1	104.59880	39.10930	−5.53030	−8.13940
C–S–O1	110.39040	68.40920	−13.86760	−14.61270

Table 3 (continued)

Bond term	b_0	k_2	k_3	k_4
O1–S–O1	120.93350	94.97580	−31.42070	−21.82430
Torsion term	k_1	k_2	k_3	
C–C–O2–H2	0.00000	1.29680	−0.00250	
C–C–C–O2	0.00000	4.60110	0.00000	
O2–C–C–S	0.00000	5.39350	0.00000	
C–C–C–C	0.00000	2.17270	0.00000	
C–C–C–S	0.00000	5.84600	0.00000	
H1–C–C–O2	0.00000	0.82750	0.00000	
C–C–C–H1	0.00000	3.52320	0.00000	
H1–C–C–S	0.00000	4.35020	0.00000	
C–C–S–O1	0.00000	1.34190	−0.21460	
H1–C–C–H1	0.00000	1.92790	0.00000	
Out-of-plane harmonic term	k			
C–C–C–O2	16.56280			
C–C–C–S	1.91800			
C–C–C–H1	11.59940			
Bond–bond cross-coupling	k			
C–O2–H2	1.54430			
C–C–O2	97.56520			
C–C–C	164.60150			
C–C–S	14.54880			
C–C–H1	31.98000			
C–S–O1	19.76380			
O1–S–O1	36.04040			
Bond–angle cross-coupling	k			
C–O2–H2	45.01050			
H2–O2–C	28.32850			
O2–C–C	47.82050			
C–C–O2	−40.26950			
C–C–C	−3.52030			
C–C–S	−92.02490			
S–C–C	88.26870			
C–C–H1	−50.18690			
H1–C–C	14.36780			
C–S–O1	−23.49370			
O1–S–C	38.60260			
O1–S–O1	45.76900			
Lennard–Jones term	r^0	ε		
S	4.05960	0.22500		
O1	3.38640	0.15300		
O2	3.43740	0.15300		
C	4.05960	0.06300		
H1	2.77440	0.02700		
H2	2.77440	0.02700		
Partial charge	q			
S	1.3864			
O1	−0.7237			
O2	−0.6579			
C	−0.1102			

Table 3 (continued)

Bond term	b_0	k_2	k_3	k_4
C(1)	−0.2153			
C(2)	0.3686			
H1	0.1102			
H2	0.2893			

Table 4 Developed CFF-type force field parameters for hydronium, as shown in Fig. 3c

Bond term	b_0	k_2	k_3	k_4
Oh–Hh	0.99280	501.76250	−1003.52510	1170.77920
Angle term	θ_0	k_2	k_3	k_4
Hh–Oh–Hh	105.04630	50.16820	−7.32400	−10.45850
Out-of-plane harmonic term	k			
Hh–Oh–Hh–Hh	7.03660			
Bond–bond cross-coupling	k			
Hh–Oh–Hh	−7.90870			
Bond–bond cross-coupling	k			
Hh–Oh–Hh	18.03840			
Lennard–Jones term	r^0	ε		
Oh	3.29870	0.07920		
Hh	2.77440	0.02700		
Partial charge	q			
Oh	−0.5495			
Hh	0.5165			

References

1. Carrette L, Friedrich KA, Stimming U (2001) Fuel cells—fundamentals and applications. Fuel Cells 1:5–39
2. Doyle M, Rajendran G (2003) Perfluorinated membranes in fuel cell technology and applications. In: Vielstich W, Lamm A, Gasteiger HA (eds) Handbook of fuel cells, vol. 3. Wiley, Chichester, pp 351–395
3. Paddison SJ (2003) First principles modeling of sulfonic acid based ionomer membranes in fuel cell technology and applications. In: Vielstich W, Lamm A, Gasteiger HA (eds) Handbook of fuel cells, vol. 3. Wiley, Chichester, pp 396–411
4. Nakano M, Yoshitake M (2003) Composite perfluorinate membranes in fuel cell technology and applications. In: Vielstich W, Lamm A, Gasteiger HA (eds) Handbook of fuel cells, vol. 3. Wiley, Chichester, pp 412–419
5. Kreuer KD (2003) Hydrocarbon membranes in fuel cell technology and applications. In: Vielstich W, Lamm A, Gasteiger HA (eds) Handbook of fuel cells, vol. 3. Wiley, Chichester, pp 420–435
6. Zawodzinski TA, Neeman M, Sillerud LO, Gottesfeld S (1991) J Phys Chem B 95:6040–6047
7. Saito M, Tsuzuki S, Hayamizu K, Okada T (2006) J Phys Chem B 110:24410–24417
8. Yeo RS (1983) J Electrochem Soc 130:533–538
9. Uosaki K, Okazaki K, Kita H (1990) J Electrochem Soc 287:163–169
10. Thompson EL, Capehart TW, Fuller TJ, Jorne J (2006) J Electrochem Soc 153:A2351–A2362
11. Mohameda HFM, Ito K, Kobayashi Y, Takimoto N, Takeoka Y, Ohira A (2008) Polymer 49:3091–3097
12. Ogumi Z, Takehara Z, Yoshizawa S (1984) J Electrochem Soc 131:769–773
13. Ogumi Z, Takehara Z, Yoshizawa S (1985) J Electrochem Soc 132:2601–2605
14. Büchi FN, Wakizoe M, Srinivasan S (1996) J Electrochem Soc 143:2601–2605
15. Zawodzinski TA, Derouin C, Radzinski S, Sherman RJ, Smith VT, Springer TE, Gottesfeld S (1993) J Electrochem Soc 140:1041–1047
16. Kinumoto T, Inaba M, Nakayama Y, Ogata K, Umebayashi R, Tasaka A, Iriyama Y, Abe T, Ogumi Z (2006) J Power Sources 158:1222–1228
17. Pozio A, Silva RF, Francesco M, Giorgi L (2003) Electrochim Acta 48:1543–1549
18. Aoki M, Uchida H, Watanabe M (2005) Electrochem Commun 7:1434–1438
19. Zaidi SMJ, Mikhailenko SD, Robertson GP, Guiver MD, Kaliaguine S (2000) J Membr Sci 173:17–34
20. Gil M, Ji XL, Li XF, Na H, Hampsey JE, Lu YF (2004) J Membr Sci 234:75–81
21. Li L, Zhang J, Wang YX (2003) J Membr Sci 226:159–167
22. Hickner MA, Ghassemi H, Kim YS, Einsla BR, McGrath JE (2004) Chem Rev 104:4587–4611
23. Mauritz KA, Moore RB (2004) Chem Rev 104:4535–4585
24. HeitnerWirguin C (1996) J Membr Sci 120:1–33
25. Kreuer KD, Paddison SJ, Spohr E, Schuster M (2004) Chem Rev 104:4637–4678
26. Kim MH, Glinka CJ, Grot SA, Grot WG (2006) Macromolecules 39:4775–4787
27. Schmidt-Rohr K, Chen Q (2008) Nat Mater 7:75–83

28. Rubatat L, Rollet AL, Gebel G, Diat O (2002) Macromolecules 35:4050–4055
29. Gebel G, Lambard J (1997) Macromolecules 30:7914–7920
30. Paddison SJ, Elliott JA (2005) J Phys Chem A 109:7583–7593
31. Paddison SJ, Zawodzinski TA (1998) Solid State Ion 113:333–340
32. Eikerling M, Paddison SJ, Pratt LR, Zawodzinski TA (2003) Chem Phys Lett 368:108–114
33. Roudgar A, Narasimachary SP, Eikerling M (2008) Chem Phys Lett 457:337–341
34. Cui S, Liu J, Selvan ME, Keffer DJ, Edwards BJ, Steele WV (2007) J Phys Chem B 111:2208–2218
35. Cui S, Liu J, Selvan ME, Paddison SJ, Keffer DJ, Edwards BJ (2008) J Phys Chem B 112:13273–13284
36. Devanathan R, Venkatnathan A, Dupuis M (2007) J Phys Chem B 111:8069–8079
37. Devanathan R, Venkatnathan A, Dupuis M (2007) J Phys Chem B 111:13006–13013
38. Venkatnathan A, Devanathan R, Dupuis M (2007) J Phys Chem B 111:7234–7244
39. Jang SS, Molinero V, Cagin T, Goddard WA (2004) J Phys Chem B 108:3149–3157
40. Brandell D, Karo J, Liivat A, Thomas JO (2007) J Mol Model 13:1039–1046
41. Urata S, Irisawa J, Takada A, Shinoda W, Tsuzuki S, Mikami M (2005) J Phys Chem B 109:4269–4278
42. Kim YS, Wang F, Hickner M, McCartney S, Hong YT, Harrison W, Zawodzinski TA, McGrath JE (2003) J Polym Sci Pt B 41:2816–2828
43. Kobayashi T, Rikukawa M, Sanui K, Ogata N (1998) Solid State Ion 106:219–225
44. Kim YS, Wang F, Hickner M, Zawodzinski TA, McGrath JE (2003) J Membr Sci 212:263–282
45. Cho CG, Kim YS, Yu X, Hill M, McGrath JE (2006) J Polym Sci Pol Chem 44:6007–6014
46. Sethuraman VA, Weidner JW, Haug AT, Protsailo LV (2008) J Electrochem Soc 155:B119–B124
47. Roy A, Hickner MA, Einsla BR, Harrison WL, Mcgrath JE (2009) J Polym Sci Pol Chem 47:384–391
48. Scienomics SARL (2002) MAPS, version 3.1. Scienomics SARL, Paris
49. Maple JR, Hwang MJ, Stockfisch TP, Dinur U, Waldman M, Ewig CS, Hagler AT (1994) J Comput Chem 15:162–182
50. Sun H (1998) J Phys Chem B 102:7338–7364
51. Pozuelo J, Riande E, Saiz E, Compan V (2006) Macromolecules 25:8862–8866
52. Hu N, Chen R, Hsu A (2006) Polym Int 55:872–882
53. Aeon Technology, Inc. (2002) Direct Force Field, version 6.0. Aeon Technology, Inc., San Diego
54. Sato F, Hojo S, Sun H (2003) J Phys Chem A 107:248–257
55. Becke AD (1993) J Chem Phys 98:5648–5652
56. Lee CT, Yang WT, Parr RG (1988) Phys Rev B 37:785–789
57. Miehlich B, Savin A, Stoll H, Preuss H (1989) Chem Phys Lett 157:200–206
58. Frisch MJ, Pople JA, Binkley JS (1984) J Chem Phys 80:3265–3269
59. Chirlian LE, Francl MM (1987) J Comput Chem 8:894–905
60. Plimpton S (1995) J Comput Phys 117:1–19
61. Verlet L (1967) Phys Rev 159:98–103
62. Hockney RW, Eastwood JW (1981) Computer simulation using particles. McGraw-Hill, New York
63. Nose S (1986) Mol Phys 57:187–191
64. Nose S (1984) J Chem Phys 81:511–519
65. Nose S (1984) Mol Phys 52:255–268
66. Nose S, Klein ML (1983) J Chem Phys 78:6928–6939
67. Humphrey W, Dalke A, Schulten K (1996) J Mol Graph 14:33
68. Paddison SJ, Elliott JA (2006) Phys Chem Chem Phys 8:2193–2203
69. Paddison SJ, Elliott JA (2006) Solid State Ion 177:2385–2390